Journal of Petroleum Science and Engineering 78 (2011) 201–207

Contents lists available at ScienceDirect

Journal of Petroleum Science and Engineering

journal homepage: www.elsevier.com/locate/petrol

Characterization of well skin using buildup test and radon as a tracer

C. Lin [a], T. Kuo [a,*], K. Fan [a], Y. Chen [a], C. Su [a], L. Tong [b], C. Lee [b], K. Hu [b], C. Liu [b], H. Liang [c], C. Tsai [d], C. Chiang [e]

[a] Department of Mineral and Petroleum Engineering, National Cheng Kung University, Tainan, Taiwan
[b] Green Energy & Environment Laboratories, ITRI, Hsinchu, Taiwan
[c] Exploration and Development Research Institute, CPC Corporation, Miaoli, Taiwan
[d] Department of Earth Sciences, National Cheng Kung University, Tainan, Taiwan
[e] Central Geological Survey, Ministry of Economic Affairs, Taipei, Taiwan

ARTICLE INFO

Article history:
Received 8 February 2011
Accepted 26 July 2011
Available online 6 August 2011

Keywords:
radon
skin
pressure buildup test

ABSTRACT

Pressure buildup tests are often used to determine the reservoir permeability and skin factor to quantify formation damage. However, no quantitative method is currently available for calculating the reduced permeability of the skin zone. With the help of radon measurements during the flow period preceding the buildup test, it is possible to calculate both the radius and the altered permeability in the damaged zone based on a radial composite model.

1. Introduction

Pressure buildup tests are the most frequently used transient well tests by petroleum engineers to determine the permeability and skin factor of a reservoir and well, respectively. Horner (1951) deduced the basic equation for pressure buildup analysis. The assumptions of Horner method are infinite reservoir, single-phase liquid flow and homogeneous reservoir. Horner plot is to obtain a straight line by plotting the pressure (P_w) observed during a shut-in period as a function of the logarithm of $\left(\frac{t_p + \Delta t}{\Delta t}\right)$, where t_p and Δt are the producing time and shut-in period, respectively. Petroleum engineers use the slope and intercept of the Horner plot to estimate the values of permeability and skin factor. In practice, we find that most wells have reduced permeability near the wellbore resulting from drilling, completion and/or production operations. Van Everdingen (1953) introduced the skin factor to account for the additional pressure drop at a damaged well compared to that at an undamaged well.

Hawkins (1956) viewed the skin factor with a damaged zone of reduced permeability (k_s) and beyond that the unaltered permeability (k). Fig. 1 shows a radial composite model with a skin zone which is induced by formation damage. The permeability varies in a step-like fashion in the radial direction away from the well. Hawkins (1956) also defined the skin factor (S) in terms of the properties of the damaged zone as follows.

$$S = \left(\frac{k}{k_s} - 1\right) \ln\left(\frac{r_s}{r_w}\right) \quad (1)$$

where r_w is the radius of well; r_s is the radius of skin zone; k_s is the reduced permeability of skin zone; k is the formation permeability. If a well is damaged ($k_s < k$), skin factor (S) will be positive. The greater the contrast between k_s and k and the deeper into the formation the damage extends, the larger the numerical value of skin factor (S). Because both the reduced permeability (k_s) and radius of the skin zone (r_s) are unknown, Eq. (1) is only limited to qualitative applications.

This paper presents a quantitative method to calculate both the reduced permeability (k_s) and radius of the skin zone (r_s) for characterizing the skin zone based on a radial composite model. The quantitative method requires radon measurements during the flow period preceding the pressure buildup test. The radius of skin zone (r_s) can be estimated with radon data (Chen et al., 2010). Conventionally, the reservoir permeability (k) and skin factor (S) are determined from pressure buildup test using the Horner method. Combining the use of radon measurement and pressure buildup test, the altered permeability in the damaged zone (k_s) can be calculated using Eq. (1). The application of radon measurements with pressure buildup tests is also presented with the help of a case study at IC-09 well of Chingshui geothermal field (Taiwan).

2. Chingshui geothermal field

The Chingshui geothermal field is an area of hot springs along the Chingshui River, in the north-east of Taiwan, approximately 20 km southwest of Lotung (Fig. 2). The Chingshui geothermal area is located on a monocline structure, which is cut internally by numerous thrust faults that are lightly curved, and essentially trend NE–SW parallel to the bedding; the most important ones are the Tashi, Hsiaonanao and Hanhsi faults, shown in Fig. 3 (Hsiao and Chiang, 1979; Su, 1978). In

* Corresponding author.
E-mail address: mctkuobe@mail.ncku.edu.tw (T. Kuo).

0920-4105/$ – see front matter.
doi:10.1016/j.petrol.2011.07.009

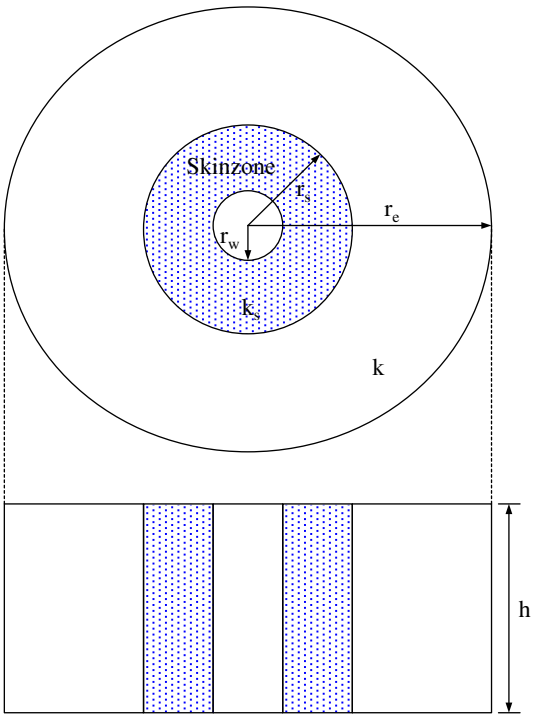

Fig. 1. A composite system with skin zone (r_w is the radius of well; r_s is the radius of skin zone; r_e is the radius of external boundary; h is the formation thickness; k_s is the reduced permeability of skin zone; k is the formation permeability).

the field itself, along the Chingshui River, there is the normal, N–S striking Chingshuihsi fault. Active tectonic movements most likely created the numerous faults and well-developed fractures around the Chingshui geothermal area. The best developed fractures in the slates are found near the most convex part of the Hsiaonanao fault along the Chingshui River.

The reservoir is within the Lushan Formation of Miocene age. The Lushan Formation can be divided lithologically into the Jentse, Chingshuihu, and Kulu Members. In general, the Jentse Member is composed mainly of metasandstones intercalated by slates, while the Chingshuihu and Kulu Members consist mostly of slates (Hsiao and Chiang, 1979; Tseng, 1978). Geothermal production at Chingshui is largely from a fracture zone in the steeply dipping Jentse Member (Hsiao and Chiang, 1979).

Based on quantitative analysis of the geophysical data together with knowledge of the geology in the Chingshui area (Tong et al., 2008), Fig. 4 shows a 3-D view of the fault systems in the vicinity of Chingshui. The geothermal reservoir, with a NW–SE trend and about 1.5 km in length, might be associated with the fracture zone of the Chingshuihsi fault and is bounded by the C-fault and the Xiaonanao fault in the north and south, respectively. The geothermal reservoir is clustered with feed zones, which are confined in an area 260 m in width, N21°W, and dip 80° to the NE.

The casing program for well IC-09 was 50.8 cm (20 in.) conductor, 34 cm (13-3/8 in.) surface casing, 24.4 cm (9-5/8 in.) production casing, and 17.8 cm (7 in.) slotted liner. The production interval is from 539 to 2086 m. The wellbore radius in the production interval is 10.8 cm (8-1/2 in.).

3. Pressure buildup test analysis of well IC-09

A flow test followed by buildup was conducted on Well IC-09 from 16:40, May 14, 2008 to 8:20, May 16, 2008. The pressure buildup test started on 20:15, May 15, 2008 after the well produced for a total flowing time of 1655 min ($t_p = 27.6$ hr) with an average total flow rate at 24.4 ton/hr ($q = 585.6$ ton/D). The flowing bottom-hole

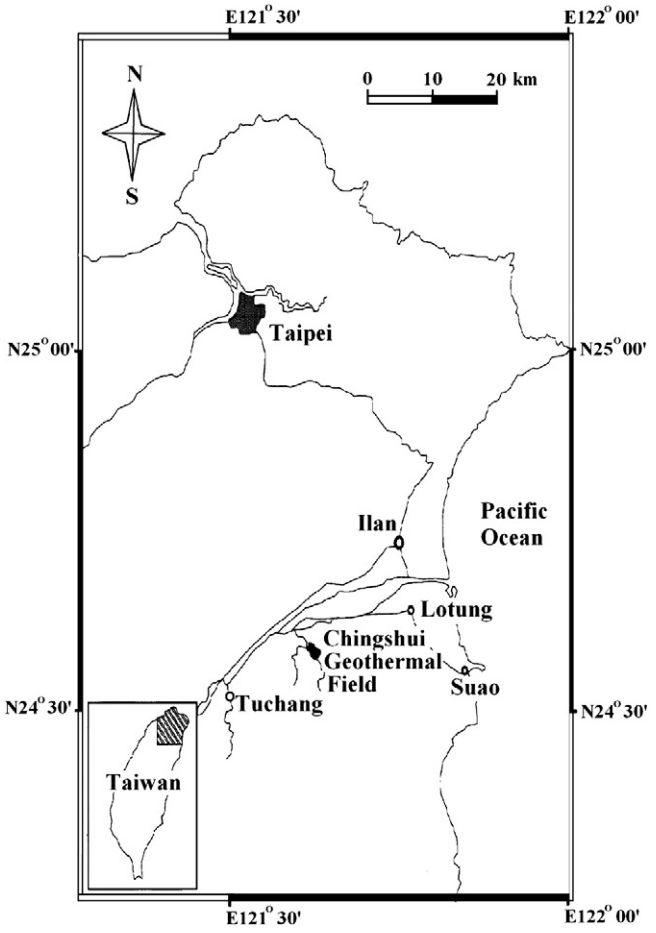

Fig. 2. Locations of the Chingshui geothermal area, Taiwan.

pressure just before well shut-in was measured at 896 psig (P_{wf}) at a depth of 1300 m. The pressure gauge was pulled out of hole on 8:20, May 16, 2008.

Pressure buildup test was analyzed by Horner plot method (Bourdet et al., 1989; Earlougher, 1977; Jeirani and Mohebbi, 2006; Lee, 1982; Matthews and Russell, 1967). Fig. 5 is the Horner plot for the buildup test. Using the slope of the straight line on Horner plot (m), the permeability-thickness product (kh) was calculated as follows.

$$kh = \frac{162.6\, q\, \mu\, B_w}{m} \tag{2}$$

The skin factor (S) was calculated as follows.

$$S = 1.1513\left[\frac{P_{1hr} - P_{wf}(\Delta t = 0)}{m} - \log\left(\frac{kh}{\phi \mu h c_t r_w^2}\right) + 3.2275\right] \tag{3}$$

where k is permeability, md; h is formation thickness, ft; q is flow rate, ton/D; μ is viscosity, cp; B_w is specific volume at reservoir conditions, reservoir bbl/ton; m is Horner Plot slope, psig/cycle; ϕ is porosity; c_t is compressibility of fluid, psi^{-1}; P_{1hr} is pressure when Horner Plot $\Delta t = 1$ hr, psig; P_{wf} is instant pressure at 1300 m depth when wellhead close, psig; r_w is production hole radius, ft.

Table 1 shows the parameter values used in the analysis. To make estimate of uncertainty in the kh product and skin, the approximate start of semi-log straight line was slightly altered. Fig. 5a, b and c shows that the corresponding slope (m) is 11.75, 12.35, and 8.33 psi/cycle for the start of semi-log straight line at $\Delta t = 300$, 400, and 500 min, respectively. The permeability-thickness product (kh)

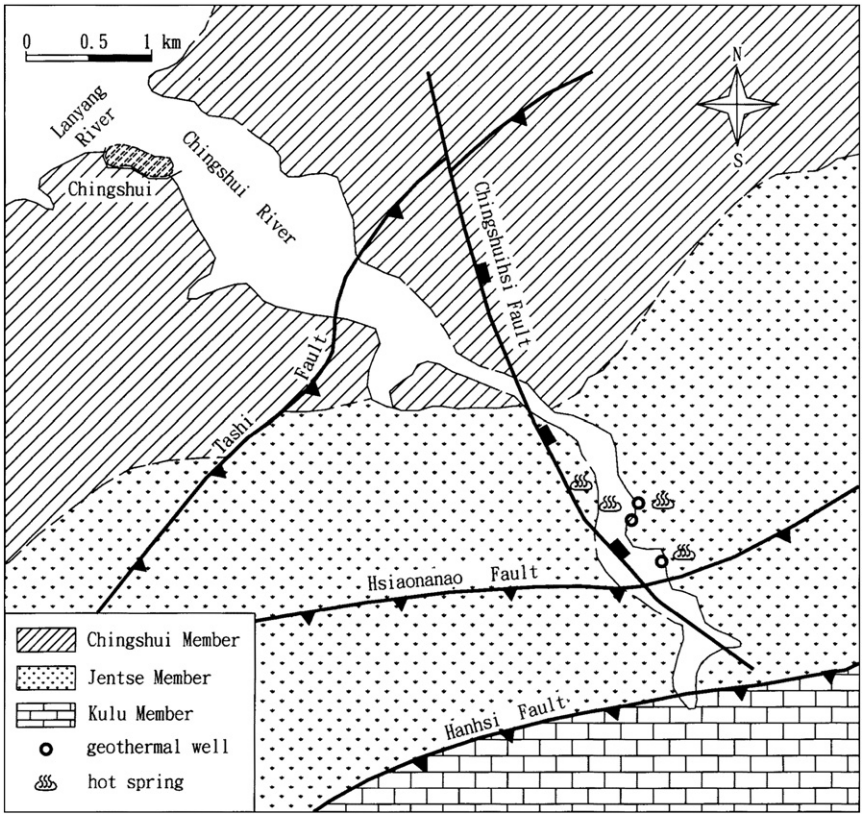

Fig. 3. Geological map of the Chingshui geothermal area showing the Chingshuihu, Jentse, and Kulu members of the Miocene Lushan Formation. Triangles and rectangles indicate the up-dipped sides of the reverse faults and the direction of dip of the normal fault, respectively.

was calculated at 7966 ± 1850 md-ft from the pressure buildup test. The high skin factor ($S = 79.8 \pm 19.9$) determined from the pressure buildup test supports that scale deposited in the reservoir.

Fig. 6 shows the log–log plot of buildup data and pressure derivative. The log–log data plot is a valuable tool for recognizing wellbore storage and identifying the infinite-acting radial flow regime. As a rule of thumb, the approximate start of semi-log straight line usually occurs about one and a half log cycles in time from the top of unit-slope straight line. The approximate start of semi-log straight line can be estimated at about 300 min (Fig. 6).

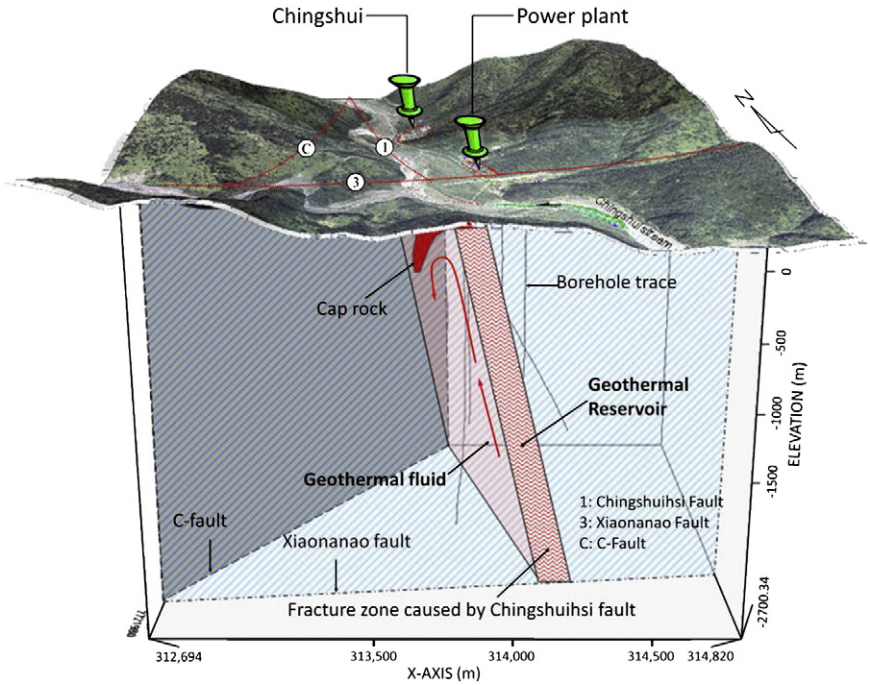

Fig. 4. The geothermal conceptual model of the Chingshui area. The geothermal reservoir might be associated with the fracture zone of the Chingshuihsi fault, and it is bounded by the C-fault and the Xiaonanao fault in the north and south, respectively.

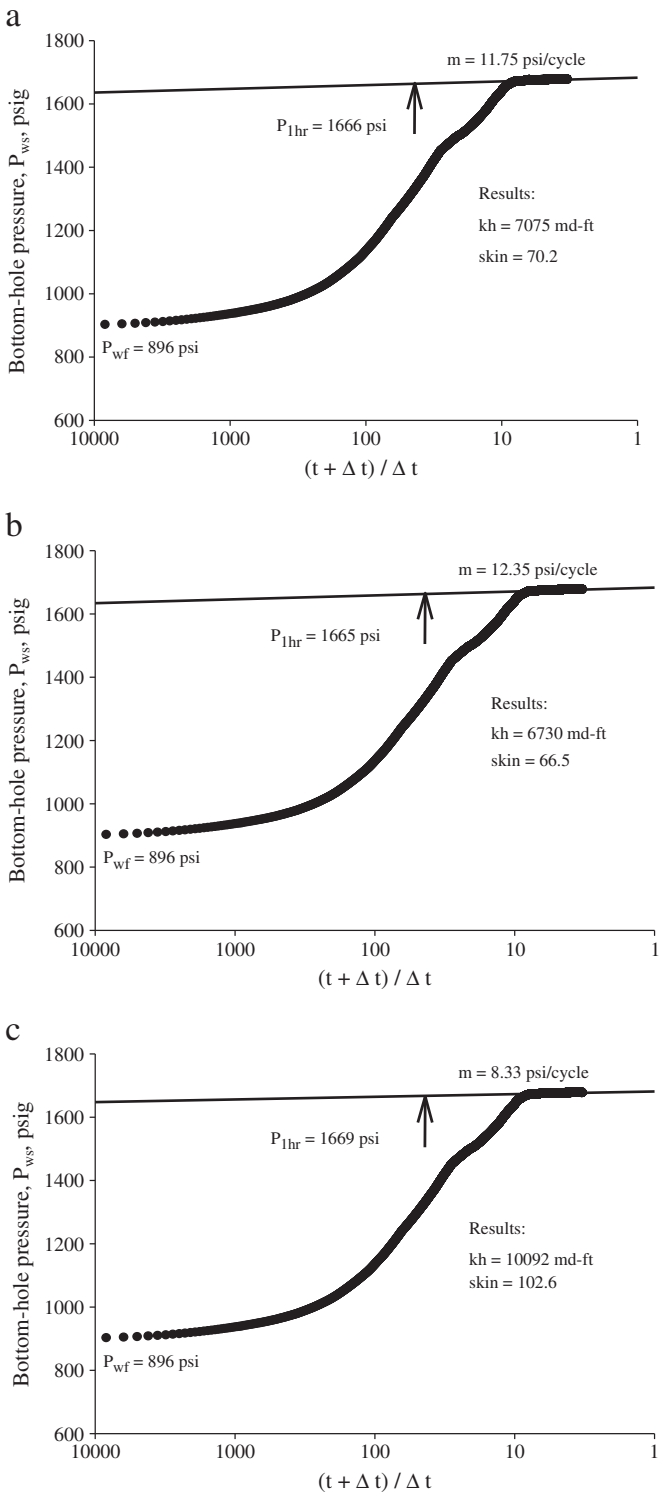

Fig. 5. The Horner plot of pressure buildup data for well IC-09. The start of semi-log straight line at (a) $\Delta t = 300$ min, (b) $\Delta t = 400$ min, and (c) $\Delta t = 500$ min.

4. Radon measurements and interpretation

From April 25, 2008, a multi-rate production test was conducted for well IC-09 in five stages with the production rate at 41.3, 32.2, 27.4, 20.2 and 34.2 ton/hr, respectively. Due to the well clean-up after work-over, radon concentration was not measured for the first flow rate (41.3 ton/hr). Radon concentration was measured in the non-condensable gases about 20 hr after each production rate started except the first flow rate. Radon measurements were conducted for a period ranging from 2 to 4 hr. In order to obtain at least four counting data points for each production rate, the time interval to record counting data was 30 min. Radon-222 concentration was measured by SARAD RTM2100 (SARAD GmbH, Germany). The instrument was operated in the 'fast mode' which excludes the detection of polonium-214 fraction. The measurement range of this instrument is from 1 Bq/m^3 to 10 MBq/m^3 for radon-222.

Table 1
Input parameters used in the pressure buildup test analysis.

Parameters	Parameter values
Total compressibility (psi^{-1}), c_t	0.00138
Viscosity (cp), μ	0.12
Specific volume at reservoir conditions (bbl/ton), B_w	1.188*35.3/5.61
Specific volume at reservoir conditions (m^3/ton), B	1.188
Porosity-thickness product (ft), ϕh	12.47
Wellbore radius (ft), r_w	0.5*8.5/12
Flow-rate (ton/D), q	26.1*24
Flowing time (hr), t_p	290.3
Flowing bottom-hole pressure (psig), P_{wf}	652

Table 2 shows the measured values of radon concentration during the flow tests of well IC-09. The measured radon concentrations before breakthrough were 67.8 ± 26.5, 63.5 ± 36.7, and 41.4 ± 21.9 Bq/m^3 with a production rate at 32.2, 27.4, and 20.2 ton/hr, respectively. The radon-222 concentration broke through at 653 Bq/m^3. The measured radon concentrations after breakthrough increased as a step function from background to 983 ± 65 Bq/m^3 with a production rate at 34.2 ton/hr, respectively.

Fig. 7 shows that the radon-222 concentration increases as a step function of production time and cumulative production during the flow tests of well IC-09 at the Chingshui geothermal field. The observed behavior of radon-222 activity in Fig. 7 implies that the reservoir consists of two sections of rocks (Fig. 1). One with significant emanating power of radon and the other with essentially zero emanating power due to the carbonate scales deposited in the skin zone near the well. Fig. 7 also shows that the radon-222 activity in the non-condensable gases was measured at 54 ± 29 and 983 ± 65 Bq/m^3 for the geothermal water inside and outside the skin zone, respectively.

The partial pressure of CO_2 in subsurface water of the Chingshui geothermal field is high ranging from 30 to 90 atm at depths between 1500 and 2000 m (Chen 1985). Well IC-09 was produced with the pressure drawdown exceeding the flash pressure in the reservoir. As CO_2 flashed off from the geothermal water, carbonate scales formed and deposited in the skin zone near the well. Scale samples from well

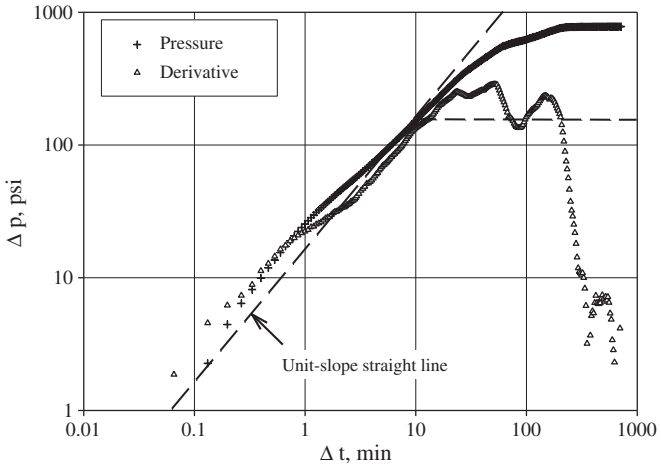

Fig. 6. The log–log plot of buildup data and pressure derivative for well IC-09.

Table 2
Multi-rate production test of Chingshui well IC-09.

Production rate (ton/hr)	Temperature (°C)	Enthalpy (kcal/kg)	Measured radon concentration (Bq/m^3)	Predicted radon concentration based on plug-flow model (Bq/m^3)
41.3	151	213		
32.2	151	201	62.7, 104.8, 41.7, 62.0 (67.8 ± 26.5)	54 ± 29[a]
27.4	161	190	42.1, 42.1, 63.0, 127.2, 43.0 (63.5 ± 36.7)	
20.2	168	202	23.0, 46.1, 43.4, 43.5, 21.5, 42.9, 88.6, 22.5 (41.4 ± 21.9)	
34.2	146	223	653, 969, 1073, 1028, 922, 927 (929 ± 147)	983 ± 65[b]

[a] Predicted concentration is average and standard deviation of 17 radon measurements before breakthrough.
[b] Predicted concentration is average and standard deviation of 5 radon measurements after breakthrough.

IC-09 were analyzed using powder x-ray diffraction (Table 3). The mineral species identified in the scale samples are calcite, aragonite, ankerite, strontianite, quartz, chlorite, illite, and feldspar. The major minerals are carbonate scales (calcite, aragonite, ankerite, and strontianite). The calcium–carbonate scales (calcite and aragonite) represent about 60% of total weight. It is hypothesized that the carbonate scales cover the surface of rocks in the skin zone as shown in Fig. 1. Because of radon's short recoil length (3×10^{-8} m), only atoms produced at the surface of rock grains are released to the surrounding geothermal water (Nazaroff, 1992; Tanner, 1964). Thus, the emanating power of radon is significantly reduced in the skin zone and is essentially zero in the skin zone.

5. Characterization of well skin

In practice, most wells have reduced permeability near the wellbore resulting from drilling, completion and/or production operations. Petroleum engineers use the skin factor to account for the additional pressure drop at a damaged well compared to that at an undamaged well (Van Everdingen, 1953). Hawkins (1956) viewed the skin factor with a damaged zone of reduced permeability and beyond that the unaltered permeability. Fig. 1 shows a radial composite system which is induced by formation damage near the well with carbonate scales. The fluid residence time (τ) in the skin zone (Fig. 1) can be defined as follows.

$$\tau = \frac{\pi r_s^2 \phi h}{qB} \tag{4}$$

where τ is the residence time of skin zone, D; r_s is the radius of skin zone, m; ϕh is the porosity-thickness product, m; q is flow rate, ton/D; B is the specific volume of geothermal water at reservoir conditions, m^3/ton. The numerator is the pore volume of the skin zone and the denominator is the flow rate of the well. Assume a zero emanating power of radon in the skin zone and a plug flow model, there is a simple relation between the residence time in the skin zone and the steady-state radon-222 concentration at the measurement well as follows (D'Amore et al., 1978; Kruger et al., 1977; Stoker, 1975).

$$N = N_0 e^{-\lambda\tau} \tag{5}$$

where N and N_0 are the radon-222 concentration at the measurement well and the source, respectively, λ is the decay constant of radon-222 ($\lambda = 0.182$ D^{-1}). According to Eq. (4), the residence time of the skin zone increases as the distance between the source of the radon and the measurement well (or, the radius of skin zone) increases. Based on Eq. (5), the steady-state radon-222 concentration at the measurement well decreases when the residence time of the skin zone increases. As the distance between the source of the radon and the measurement well increases, the steady-state radon-222 concentration at the measurement well decreases.

The emanating power of radon from aquifer rocks is significantly reduced by the carbonate scales. Assume that the emanating power of radon from aquifer rocks is zero in the skin zone and the emanating power of radon increases as a step function in the radial direction away from the well (Fig. 1). The pore volume of the skin zone shown in Fig. 1 is defined as $\pi r_s^2 \phi h$ where r_s is the radius of skin zone, m; ϕh is the porosity-thickness product, m. Assuming a plug flow model (Levenspiel, 1972; Smith, 1970), the radon-222 concentration increases as a step function at breakthrough after one pore-volume of the formation fluid has been purged out of the skin zone. Based on the observed radon-222 concentration as a function of cumulative production, we can identify the breakthrough and calculate the size of the skin zone (Chen et al. 2010).

Table 2 and Fig. 7 show that the radon-222 concentration broke through at 653 Bq/m^3 during the multi-rate production test of Chingshui well IC-09. Based on the plug flow model, the predicted radon concentration before breakthrough was estimated at 54 ± 29 Bq/m^3

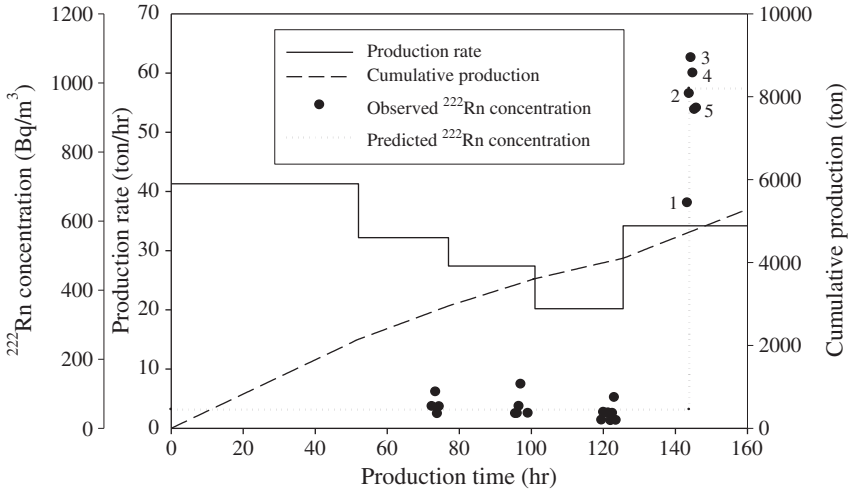

Fig. 7. Radon-222 concentration, production rate, and cumulative production versus production time for multi-rate test of well IC-09.

Table 3
Mineral species and composition identified in scales samples from well IC-09 using x-ray diffraction.

Sample	Sample depth (m)	Calcite	Aragonite	Ankerite	Strontianite	Quart	Illite	Chlorite	Feldspar	Total (weight %)
CS1	0–50	18.44	28.56	20.74	32.24	0.02				100.00
CS2	50–100	21.25	35.58	9.16	33.88	0.14				100.00
CS3	100–150	13.79	42.67	8.55	33.07	1.93				100.00
CS4	150–200	18.79	40.28	7.01	33.06	0.86				100.00
CS5	200–250	13.63	45.15	6.21	34.10	0.93				100.00
CS6	250–300	8.20	50.18	8.13	31.98	1.51				100.00
CS7	300–350	35.10	23.04	8.46	32.34	1.06				100.00
CS8	350–400	8.05	49.27	6.88	32.35	3.45				100.00
CS9	400–450	19.57	52.85	12.59	13.82	1.16				100.00
CS10	450–500	56.50	16.61	12.87	13.53	0.49				100.00
CS11	928	76.10	8.51	10.77	3.85	0.77				100.00
CS12	957	77.92	7.29	10.68	3.88	0.22				100.00
CS13	1300	48.14	16.84	11.48	14.87	2.30	1.77	3.62	0.98	100.00
CS14	1311	18.48	31.98	9.53	14.52	5.40	4.66	10.48	4.95	100.00
CS15	1436	19.13	39.15	7.42	32.87	1.43				100.00
CS16	1605	35.13	27.76	9.42	27.17	0.52				100.00
CS17	1960	38.68	21.72	13.03	14.76	2.15	2.32	6.42	0.93	100.00
CS18	1980	36.21	23.15	16.80	10.49	3.27	3.43	6.63		100.00
CS19	2010–2020	49.74	18.94	14.54	9.78	1.72	1.13	3.23	0.91	100.00
CS20	2040–2060	21.19		12.74	4.42	38.56	4.62	18.46		100.00

using 17 radon measurements shown in Table 2. The predicted radon concentration after breakthrough was estimated at 983 ± 65 Bq/m^3 using 5 radon measurements shown in Table 2.

Chen et al. (2010) applied radon as a natural tracer to estimate the size or radius of skin zone using the plug flow model as follows.

$$Q = \frac{\pi r_s^2 \phi h}{B} \tag{6}$$

where Q is the cumulative production of geothermal water at radon breakthrough, ton; r_s is the radius of skin zone, m; ϕh is the porosity-thickness product, m; B is the specific volume of geothermal water at reservoir conditions, m^3/ton. The radon-222 concentration broke through at 653 Bq/m^3 with a cumulative production (Q) of 4738 ton of geothermal water. The values of porosity-thickness product (ϕh) and specific volume of geothermal water at reservoir conditions (B) were estimated at 3.8 m and 1.188 m^3/ton, respectively (Cheng et al., 2010; Fan et al., 2005). Using Eq. (6), the radius of skin zone (r_s) was estimated at 21.7 m.

Given the radius of wellbore ($r_w = 0.108$ m), the radius of skin zone ($r_s = 21.7$ m) estimated from radon measurements, and the permeability-thickness product ($kh = 2430$ md-m) and skin factor ($S = 79.8$) determined from pressure buildup test, Eq. (1) was used to calculate the reduced permeability-thickness product of skin zone ($k_s h$) at 151 md-m. If the thickness of Chingshui geothermal reservoir is known, it is possible to separate the average permeability-thickness product into effective permeability and net thickness. Based on the geothermal conceptual model of the Chingshui area (Tong et al., 2008), the thickness of Chingshui geothermal reservoir is estimated to be 2300 m. The reservoir permeability and the altered permeability of skin zone are approximately 1.06 md and 0.066 md, respectively.

6. Conclusions

Currently there is no quantitative method available to estimate the altered permeability of skin zone. Direct measurement of the altered permeability of skin zone is difficult. A quantitative method has been presented to calculate the radius and the altered permeability in the damaged zone based on a radial composite model. The method requires radon measurements during the flow period preceding the buildup test.

The observed radon behavior during the flow tests of well IC-09 implied a radial composite system which is induced by formation damage with carbonate scales in the skin zone. The high skin factor ($S = 78.5$) determined from pressure buildup test also supports the formation damage resulting from carbonate scales in the skin zone. In many cases skin is caused by invasion of drilling fluids, plugging of perforations, or other factors. The applicability of radon is not limited only to cases with calcite deposition. When the emanating power of radon is significantly reduced in the skin zone, monitoring natural radon during the flow period preceding the buildup test can be a helpful tracer to diagnose the formation damage near the well.

Nomenclature

B	Specific volume at reservoir conditions, m^3/ton
B_w	Specific volume at reservoir conditions, bbl/ton
c_t	Total compressibility, psi^{-1}
k	Formation permeability, md
k_s	Reduced permeability of skin zone, md
kh	Permeability-thickness product, md-ft
m	Slope of the straight line on Horner plot, psig/cycle
N	Radon-222 concentration at the well, Bq/m^3
N_0	Radon-222 concentration at the source, Bq/m^3
P_{1hr}	Static bottom-hole pressure on the straight line of Horner plot when $\Delta t = 1$ hr, psig
P_w	Static bottom-hole pressure, psig
P_{wf}	Flowing bottom-hole pressure before shut-in, psig
q	Flow rate, ton/hr or ton/D
Q	Cumulative production of geothermal water, ton
r_s	Radius of skin zone, m
r_w	Radius of well, ft or m
S	Skin factor
Δt	Shut-in period, hr
t_p	Producing time, hr

Greek letters

λ	Decay constant of radon-222, D^{-1}
μ	Viscosity, cp
τ	Residence time in skin zone, D
ϕh	Porosity-thickness product, ft or m

Acknowledgments

Support by the National Science Council and the Bureau of Energy, Ministry of Economic Affairs of Taiwan (NSC 99-ET-E-006-011-ET and

NSC 100-ET-E-006-007-ET) is appreciated. The authors are also grateful to Taiwan Radiation Monitoring Center for laboratory support.

References

Bourdet, D., Ayoub, J.A., Plrard, Y.M., 1989. Use of pressure derivative in well-test interpretation. SPE Formation Evaluation 4, 293–302.
Chen, C.H., 1985. Chemical characteristics of thermal waters in the central range of Taiwan. R.O.C. Chemical Geology 49, 303–317.
Chen, Y., Kuo, T., Fan, K., Liang, H., Tsai, C., Chiang, C., Su, C., 2010. Radon measurements at IC-09 well of Chingshui geothermal field (Taiwan): a case study. Radiation Measurements 46, 270–276.
D'Amore, F., Sabroux, J.C., Zettewoog, P., 1978. Determination of characteristics of steam reservoirs by radon-222 measurement in geothermal fluids. Pageoph 177, 253–261.
Earlougher Jr., R.C., 1977. Advances in Well Test Analysis, 2nd edition. Society of Petroleum Engineers of AIME, New York.
Fan, K.C., Kuo, M.C.T., Liang, K.F., Lee, C.S., Chiang, S.C., 2005. Interpretation of a well interference test at the Chingshui geothermal field, Taiwan. Geothermics 34, 99–118.
Hawkins Jr., M.F., 1956. A note on the skin effect. Transaction of AIME 207, 356–357.
Horner, D.R., 1951. Pressure build-up in wells. Third World Pet. Cong., E.J, Brill, II: 503.
Hsiao, P.T., Chiang, S.C., 1979. Geology and geothermal system of the Chingshui-Tuchang geothermal area, Ilan, Taiwan. Petroleum Geology of Taiwan 16, 205–213.
Jeirani, Z., Mohebbi, A., 2006. Estimating the initial pressure, permeability and skin factor of oil reservoirs using artificial neural networks. Journal of Petroleum Science amd Engineering 50, 11–20.
Kruger, P., Stoker, A., Umana, A., 1977. Radon in geothermal reservoir engineering. Geothermics 5, 13–19.
Lee, J., 1982. Well Testing, 1st edition. Society of Petroleum Engineers of AIME, New York.
Levenspiel, O., 1972. Chemical Reaction Engineering. Wiley, New York.
Matthews, C.C., Russell, D.G., 1967. Pressure Buildup and Flow Tests in Wells. Monograph Series. Society of Petroleum Engineers of AIME, Dallas. 1.
Nazaroff, W.W., 1992. Radon transport from soil to air. Reviews of Geophysics 30, 137–160.
Smith, J.M., 1970. Chemical Engineering Kinetics, Second ed. McGraw-Hill, New York.
Stoker, A., 1975. Radon measurement in geothermal system. Engineer's Thesis, Department of Civil Engineering, Stanford University, December 1981, SGP-TR-4, p. 120.
Su, F.C., 1978. Resistivity survey in the Chingshui prospect, I-Lan, Taiwan. Petroleum Geology of Taiwan 15, 255–264.
Tanner, A.B., 1964. Radon migration in the ground: a review. In: Adams, J.A.S., Lowder, W.M. (Eds.), The Natural Radiation Environment. University of Chicago Press, Chicago, pp. 161–196.
Tong, L.T., Ouyang, S., Guo, T.R., Lee, C.R., Hu, K.H., Lee, C.L., Wang, C.J., 2008. Insight into the geothermal structure in Chingshui, Ilan, Taiwan. Terrestrial Atmosphere-Ocean Science 19, 413–424.
Tseng, C.S., 1978. Geology and geothermal occurrence of the Chingshui and Tuchang districts, Ilan. Petroleum Geology of Taiwan 15, 11–23.
Van Everdingen, A.F., 1953. The skin effect and its influence on the productive capacity of a well. Transaction of AIME 198, 171–176.